

Cite this: DOI: 10.1039/c3ob27331h

Probing deep into the interaction of a fluorescent chalcone derivative and bovine serum albumin (BSA): an experimental and computational study†

Haline G. O. Alvim,^{a,b} Emma L. Fagg,^{a,b} Aline L. de Oliveira,^{a,b} Heibbe C. B. de Oliveira,^{a,b} Sonia M. Freitas,^c Mary-Ann E. Xavier,^c Thereza A. Soares,^d Alexandre F. Gomes,^e Fabio C. Gozzo,^e Wender A. Silva*^b and Brenno A. D. Neto*^a

In the present manuscript, a novel fluorescent chalcone derivative is synthesized and its photophysical properties are fully characterized. The designed fluorophore is applied as a probe to study protein–dye interactions with bovine serum albumin. Circular dichroism gave interesting results on the thermodynamics of the interaction. NMR spectroscopy, especially relaxation measurements, revealed the atoms in the chalcone derivative that interacts with the protein upon binding. Molecular docking calculations indicate that the most favourable binding sites are near the two tryptophan residues. Furthermore, *ab initio* and DFT calculations offer insights into the reactivity and physicochemical properties of this novel fluorophore.

Received 30th November 2012,

Accepted 30th April 2013

DOI: 10.1039/c3ob27331h

www.rsc.org/obc

Introduction

It is well accepted that for a deeper understanding of a protein–drug interaction, it is necessary that one has knowledge of both the binding mode in the host biomolecule and the guest properties, *i.e.* its reactivity, photophysics and stereochemistry. The guest molecule is almost always a fluorescent probe, which allows very sensitive assays since fluorescence is by far the most sensitive of the available spectroscopic techniques for this purpose.¹ In this sense, a lot of effort is being made to rationalize the main interactions of several classes of fluorescent compounds with a plethora of proteins, as recently reviewed.² Over the years, there has been a great and increasing interest in the investigation of chalcones–BSA interactions as models to probe protein–drug interactions.^{3,4} Since HSA (human serum albumin) and BSA are ~80% homologous,⁵

HSA can also be used. Moreover, chalcones appear to interact in a similar manner with BSA and HSA.⁶ Nevertheless, there are two main advantages associated with the use of BSA, namely better stereochemical recognition (including chiral guests)⁷ and more rigid binding pockets.^{8,9}

Chalcones (1,3-diaryl-2-propen-1-ones and the derivatives of this basic structure, Fig. 1) belong to the flavonoid family, and commonly possess interesting biological activities such as anticancer, antimicrobial, antiprotozoal, antihistaminic, anti-inflammatory and many other activities, as reviewed elsewhere.^{10,11} Currently, several of these derivatives have been approved for clinical use or are already being tested in humans.¹² Beyond these attractive clinical properties, new biological activities of chalcones such as in antiblood platelets coagulation, antihemostasis and microbial resistance are currently under investigation.¹³ Additionally, fluorescent chalcones are also used in a wealth of technological applications.¹⁴ Thus, there is a continuous interest in research on this class of compounds.

It has been already revealed that proteins are one of the preferential targets for biologically active chalcones apart from

^aLaboratory of Medicinal and Technological Chemistry, University of Brasilia (IQ-UnB), Campus Universitário Darcy Ribeiro, CEP 70904970, P.O. Box 4478, Brasilia-DF, Brazil. E-mail: brenno.ipi@gmail.com

^bLaboratory for Bioactive Compounds Synthesis, University of Brasilia (IQ-UnB), Campus Universitário Darcy Ribeiro, CEP 70904970, P.O. Box 4478, Brasilia-DF, Brazil. E-mail: wender@unb.br

^cLaboratório de Biofísica, Depto de Biologia Celular (IB-UnB), Universidade de Brasília, UnB, Brasília, DF, Brazil

^dDepartment of Fundamental Chemistry, (dQF-UFPE), Av. Jornalista Anibal Fernandes, s/n – Cidade Universitaria, 50740-560, Recife-PE, Brazil

^eInstitute of Chemistry, University of Campinas, Campinas, SP, Brazil

†Electronic supplementary information (ESI) available: NMR spectra, synthetic procedures and other details are also available. See DOI: 10.1039/c3ob27331h

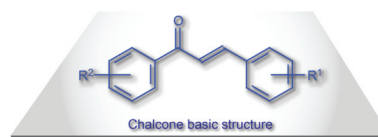


Fig. 1 The general chalcone structure.

their origin (natural or synthetic).¹³ Nevertheless, still very little is known, especially at the molecular level, about their interactions mode, *i.e.* chalcone–protein interactions.

The photophysical properties of chalcones are also of great scientific and technological interest and, as one can expect, the understanding of such properties is a sizable challenge as recently reported.^{15,16} Many of these derivatives display attractive photophysical properties such as large Stoke shifts, reasonable fluorescence quantum yields, efficient stabilizing charge-transfer processes in the excited state, large sensitivity regarding the surrounding medium, *i.e.* hydrogen bonding ability with the medium, polarity of the environment, pH tuned emissions, *etc.* Not rarely, chalcones also have the property of a dual fluorescence emission (or triple).¹⁷

The chalcone basic structure (Fig. 1) naturally leads to the idea of a donor–acceptor–donor architecture (D–A–D), in which the C=C–C=O group (Michael system) is the accepting moiety while one or both phenyl groups can act as donor(s) in the excited state (Fig. 2); thus it is reasonable to expect an efficient intramolecular (or internal) charge transfer (ICT), especially with electron donating groups attached to the phenyl moieties (*e.g.* NM₂, OMe and others) side of the scaffold as efficient electron donors. Moreover, it has been demonstrated that methoxy groups as the substituents have a beneficial effect on the fluorescence intensity of some chalcone derivatives.¹⁸ This specific molecular architecture (also known as push–pull), which include the appropriate substituents, is responsible for the fluorescent emission of chalcones,¹⁹ since its basic structure (Fig. 1, R¹ = R² = H) is virtually non-fluorescent.

We have already described interactions such as host–guest of fluorescent probes with proteins and DNA.^{20–22} More recently, we have exploited the molecular architecture of some fluorescent benzothiadiazole derivatives stabilized by ICT processes with D–A–D molecular architecture and the selective mitochondrial staining with those dyes.^{23,24} Based on our interest in the chemistry of chalcones^{25–27} and their biological applications, we describe herein the design, synthesis, properties and interactions of a fluorescent chalcone derivative with BSA. Moreover, computational calculations are also presented to understand host–guest interactions and chalcone properties at the molecular level, including the excited state.

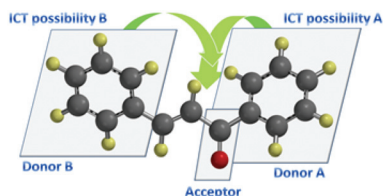


Fig. 2 Donor–acceptor–donor (D–A–D) molecular architecture (or push–pull design) of a general chalcone structure. Possible substituents in the phenyl groups, which are the chromophores responsible for the fluorescent properties, have been omitted for clarity.

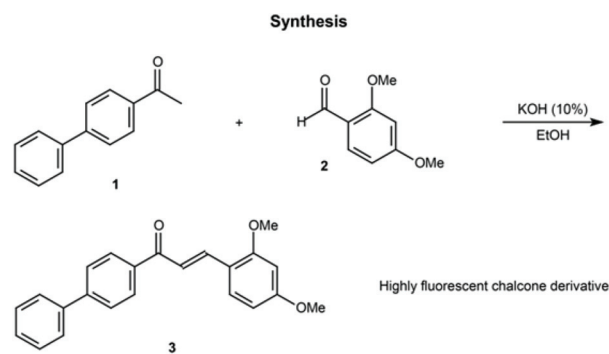
Results and discussion

Synthesis and photophysical properties

The designed fluorescent chalcone was synthesized by a Claisen–Schmidt condensation as shown in Scheme 1. The synthesized compound was rationalized by aiming at a biphenyl moiety to display an enhanced fluorescence^{28,29} and two methoxy groups to facilitate the ICT process in the excited state.³⁰ It has been already demonstrated that a biphenyl moiety has a beneficial effect on the fluorescence of a chalcone derivative.³¹ It is worth noting that the novel chalcone derivative **3** was designed and synthesized considering the molecular architecture previously presented in Fig. 2.

The photophysical properties of the novel compound was evaluated by spectrophotometric and spectrofluorimetric analyses followed by titrations with a BSA solution (phosphate buffer, pH 7.2). Initially, to investigate the ICT possibility of these new compounds, solvatochromic effects (by spectrophotometric and spectrofluorimetric analyses) were carried out, and the results are summarized in Table 1. All spectra are found in the ESI file (Fig. S1–S7†) as the dual emission values observed for some solvents. This dual emission is a consequence of a locally excited state followed by the ICT process as explored and explained elsewhere.¹⁷ This work aims to focus on the observed interactions with the biomolecule, as will be discussed in due course.

Stokes shifts are largely dependent on the solvent, and a polar protic solvent (methanol) showed the largest Stoke shift



Scheme 1 Synthesis and rationalization of the designed fluorescent chalcone derivative. Note the donor–acceptor–donor (D–A–D) molecular architecture of chalcone **3** and the purpose of each part.

Table 1 UV-Vis and fluorescence emission data (in different solvents) for **3**

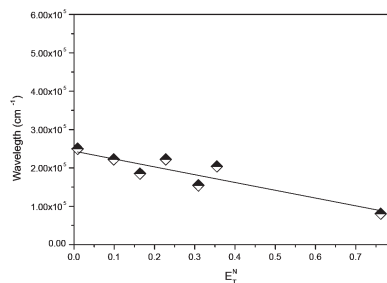
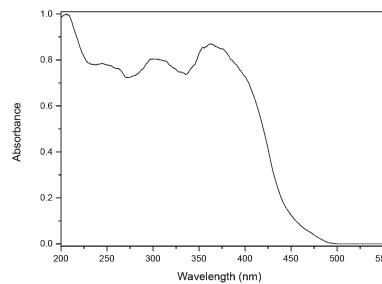
Solvent	λ_{\max} (abs) (nm)	Log ϵ (ϵ)	λ_{\max} (em) (nm)	Stokes shift (nm)
Dichloromethane	363	4.39 (24 385)	433	70
Methanol	370	4.42 (26 271)	494	124
Acetone	363	4.45 (28 348)	408	45
1,4-Dioxane	358	4.35 (22 249)	416	58
Ethyl acetate	358	4.34 (22 247)	403	45
Toluene	357	3.84 (6979)	402	45
Hexane	345	3.88 (7602)	385	40

(124 nm) (Table 1). The lowest energy absorption bands are assigned to π - π^* transitions by virtue of their large molar extinction coefficients (log ϵ values in the range of 3.84–4.45 $\text{mM}^{-1} \text{cm}^{-1}$), thus indicating an efficient ICT process of stabilization in the excited state. Both the large Stokes shift and the large molar extinction coefficients suggest a structural change in the excited state compared with the ground state, which has a direct effect on the dipole moment of the structure as will be explored in the Theoretical calculations section.³² Therefore the ICT process dictates the molecule structure in the excited state. Moreover, it is noted that there is a bathochromic shift with an increase of both the solvent polarity and the dielectric constants, consistent with an efficient ICT process, as already noticed for other chalcone derivatives previously described.³³

By using the Stokes shift values obtained with seven different solvents, it was possible to evaluate the ICT process in the first excited state using the Lippert–Mataga plot (Fig. 3) with the E_{T}^{N} solvent parameter given by Reichardt.³⁴

It is known that charge transfer states can be more stabilized upon increasing the solvent polarity (in the current case, methanol and dichloromethane gave good results); thus a linear relationship of the difference of the fluorescence maxima and absorption maxima *vs.* the solvent polarity function (Δf or E_{T}^{N}) suggests the occurrence of the internal charge transfer state and its efficiency. The linearity of the plot (Fig. 3, $R^2 = 0.91$) corroborates with an efficient ICT process, as observed for many chalcone derivatives.^{35–37}

Solid-state ultraviolet spectroscopic measurements were also performed to determine the band gap of chalcone **3** (Fig. 4). It is noted that a low band gap value is found for the synthesized compound **3** (2.49 eV), which was determined

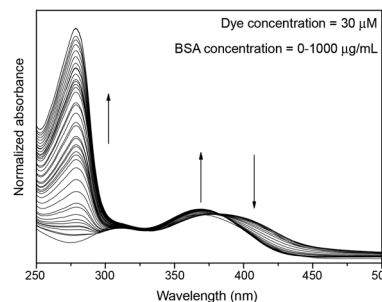
**Fig. 3** Stokes shift (cm^{-1}) of **3** *vs.* E_{T}^{N} values for the seven tested solvents. R^2 of 0.91 for the linear plot.**Fig. 4** UV-Vis (solid-state) of compound **3**. The band gap (HOMO–LUMO energy difference) was determined from the absorption edge of the solid-state spectrum (502 nm). Determined band gap $E_{\text{gap}} = 2.49$ eV.

from the absorption edge of the solid-state spectrum.³⁸ This low value of the HOMO–LUMO (band gap) difference is a consequence of the large π -extension of the conjugation and the efficiency of the mesomeric effect because of the presence of two methoxy groups in the structure. The orbital isopotential surface of both the ground and excited states of the chalcone derivative **3** were calculated and will be presented in the Theoretical calculations section.

Spectrophotometric and spectrofluorimetric titrations

Initially, a buffered solution (phosphate buffer at pH 7.2) of compound **3** was titrated with increasing BSA concentration (0–1000 $\mu\text{g mL}^{-1}$) and the results are summarized in Fig. 5.

In the absence of BSA, compound **3** showed absorption maxima at 369 nm and a large log ϵ value (4.15). Upon BSA addition, it is noted that there are a clear isosbestic point formation at 384 nm and a possible second isosbestic point at 328 nm. These observations already indicate a binding interaction between the dye and BSA (protein–dye complex formation), and the isosbestic points suggest that at least one binding mode takes place.^{39,40} Additionally, spectrophotometric titrations of dye **3** in the presence of BSA showed a slight hypsochromic shift (from 382 nm to 369 nm) of the absorption maxima showing a change in the molecular environment of the fluorophore. This observation is in full accordance with an interaction between chalcone **3** and the hydrophobic binding sites of BSA.⁴¹

**Fig. 5** Spectrophotometric titrations of BSA to **3** at a dye concentration of 30 μM . Arrows indicate changes in the absorption spectra upon the addition of the protein (BSA = 0–1000 $\mu\text{g mL}^{-1}$). Experiments carried out in phosphate buffer (pH = 7.2).

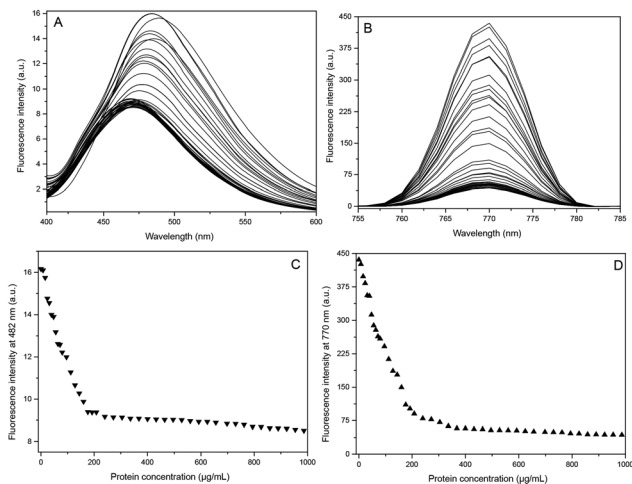


Fig. 6 Fluorimetric titration of BSA (0–1000 $\mu\text{g mL}^{-1}$) to a solution of **3** at a dye concentration of 10 μM . (A) and (B) Expansion regions. Excitation wavelength at 384 nm. Experiments carried out in phosphate buffer (pH = 7.2). Fluorescence intensity upon BSA addition at 482 nm (C) and at 770 nm (D).

The excitation wavelength for the fluorimetric titrations corresponded to the isosbestic point (384 nm), which was directly determined from the photometric titrations. All spectrofluorimetric titrations could be carried out using the dye **3** at a lower concentration (10 μM) and the results are summarized in Fig. 6.

The addition of BSA resulted in a quenching effect of the fluorescence, which decreases with the addition of the protein (Fig. 6C and 6D). Moreover, the plot of the binding isotherm from fluorimetric titrations of BSA to a solution of **3** is a sigmoidal plot in a rather large range (0–1000 $\mu\text{g mL}^{-1}$) with the correlation coefficient being 0.99 (Fig. 7), thus allowing for direct fluorimetric detection and quantification of the protein concentration in solution.

A linear correlation is noted in the fluorescence emission at 482 nm, but only in a relatively broad range (0–200 $\mu\text{g mL}^{-1}$ \approx 3.00 μM of protein concentration) with the correlation coefficient being 0.99 (Fig. 8).

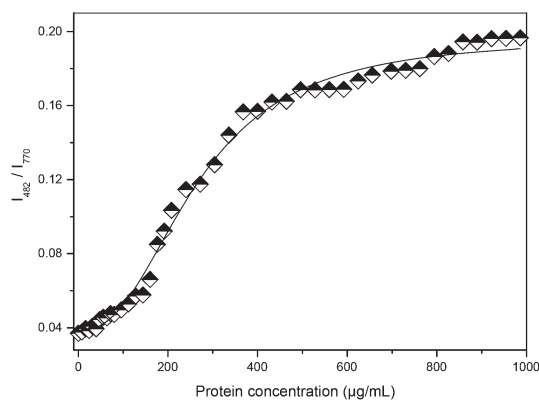


Fig. 7 Binding isotherm from fluorimetric titrations of BSA to a solution of **3** at a dye concentration of 10 μM and showing the ratiometric response (I_{482}/I_{770}) of probe **3**. Correlation coefficient 0.99.

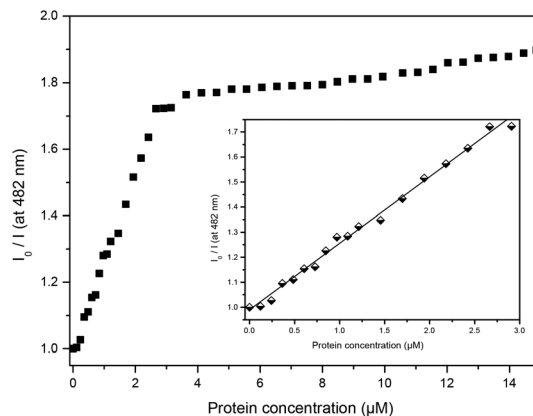


Fig. 8 I_0/I against BSA concentration (0–1000 $\mu\text{g mL}^{-1}$ \approx 0.0–15.0 μM) in phosphate buffer (pH = 7.2) and dye concentration of 10 μM . The inset represents the linear region of I_0/I against BSA concentration (0–200 $\mu\text{g mL}^{-1}$ \approx 0.0–3.0 μM).

In the linear region (0–200 $\mu\text{g mL}^{-1}$ \approx 0.0–3.0 μM), the quenching is mainly due to the dynamic process; thus a diffusion process is dominant.⁴² The Stern–Volmer constant (K_{SV}) could then be calculated according to eqn (1), where $[Q]$ is the quencher (BSA) concentration.

$$I_0/I = 1 + K_{SV} [Q] \quad (1)$$

K_{SV} showed a low value (0.27 M^{-1}) clearly indicating that the fluorophore is relatively buried in the macromolecule, and the main chromophores are inaccessible. Above these values, there is no significant change in fluorescence, thus indicating that almost all of chalcone **3** is associated with BSA, thus reaching equilibrium by forming a protein–dye complex at a concentration of $\approx 1:3$ (BSA–chalcone).

Circular dichroism spectroscopy

The association of chalcone with BSA by forming a stable complex and the structural thermostability of the complex were measured *via* near and far-UV circular dichroism spectroscopy, respectively. To investigate complex formation between BSA and chalcone **3** and its affinity, a titration study was carried out by progressive chalcone addition at a constant BSA concentration monitored by near-CD spectroscopy. A typical equilibrium binding process is shown in Fig. 9 and 10.

The CD spectra displayed three peaks: one peak positive at 382 nm and the others negative at ≈ 300 and 254 nm, with increasing CD signal as a function of compound **3** addition. The negative dichroic bands are due to the contribution of tryptophan and phenylalanine residues, and the changes in intensity correspond to structural perturbation of the residues environment induced by chalcone addition, thus indicating the proximity of **3** and tryptophan residues. On the other hand, the positive CD signal at 382 nm increased upon chalcone **3** binding in a concentration dependent manner is the indication of complex formation (host–guest), as shown in Fig. 10. At chalcone saturating concentration the CD signal tends to stabilize, thus indicating that the BSA binding process

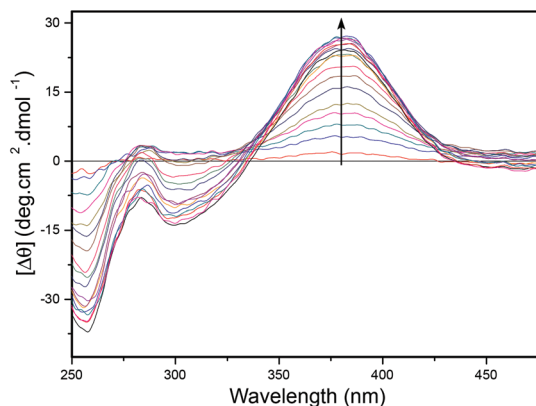


Fig. 9 Near-UV CD spectra of 3.0×10^{-5} M BSA in the presence of chalcone **3** in the concentration range of 0.5×10^{-5} to 9.0×10^{-5} M at 5 mM Tris-HCl buffer (pH = 7.5, 25 °C). The arrow indicates the CD signal increasing at 382 nm as a function of chalcone additions.

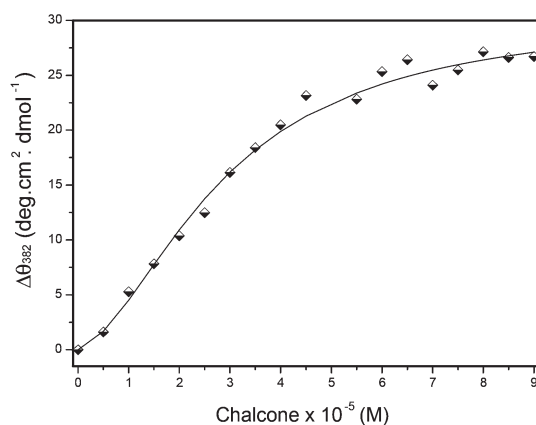


Fig. 10 Ellipticity values at 382 nm of 3.0×10^{-5} M of BSA as a function of chalcone concentration. The symbols represent experimental data while the solid line represents the fitting considering two binding sites of the BSA–chalcone association. The binding constants from the experimental data are $K_{D1} = 0.87 \pm 0.13 \times 10^{-6}$ M and $K_{D2} = 0.94 \pm 0.23 \times 10^{-7}$ M.

had reached its equilibrium at a BSA–chalcone stoichiometry of 1 : 3 (in accordance with spectrofluorimetric titrations). The binding curve (Fig. 10) was well-fitted to a non-linear model corresponding to two independent binding sites (which will be also discussed using molecular docking), one of them with higher affinity, as indicated by two equilibrium constants estimated as $K_{D1} = 0.87 \pm 0.13 \times 10^{-6}$ M and $K_{D2} = 0.94 \pm 0.23 \times 10^{-7}$ M

(see the Experimental section for details). This model indicates that almost all binding sites of BSA are occupied in a low chalcone concentration characterizing a high affinity host–guest interaction ($K_D \approx 10^{-7}$ M).

The far-UV spectra of 3.0×10^{-7} M of BSA in the absence and presence of 1.5×10^{-7} M of chalcone **3** (data not shown) were very similar presenting the characteristic band at 222 nm corresponding predominantly to α -helix structure.^{43–45} No significant changes in terms of α -helix content (data not shown) were observed, suggesting that chalcone itself does not promote considerable secondary structure alteration in BSA at 25 °C. However, the thermodynamic parameters of protein denaturation obtained from unfolding curves indicate a significant increase in the stability of BSA host–guest complex formation (Table 2).

Protein stability can be measured by changes in the Gibbs energy from the native to unfolded transition states, and can be useful to characterize its potential technological application.⁴⁶ In general, the high stability of proteins may be verified by the changes in enthalpy (>90 kcal mol⁻¹) and the Gibbs free energy (>10 kcal mol⁻¹). The value attributed to the entropy is associated with an increase in the conformational freedom of the polypeptide chain with the hydration of exposed groups in the unfolded state, whereas the enthalpy is directly related to the contribution of non-covalent interactions to the protein structure arrangement.

In this work, the thermal stability of the free and chalcone **3**-bound BSA (at pH 7.5) was assessed upon raising the temperature from 25 °C to 95 °C monitored by the dichroic signal at 222 nm. The thermal denaturation curves show the θ_{222} signal decreasing with an increase in temperature following two distinctive transitions from native to intermediate (25 °C to ≈ 75 °C) and from intermediate to unfolding states (≈ 75 °C to 92 °C). Normalized unfolding curves of both proteins (Fig. 11) indicate that these molecules melt in two independent ways in the non-two-state model, in which the second transition exhibits significantly larger thermodynamic parameters values (Table 2). It has been proposed that BSA has three homologous domains composed of several helical segments connected by unordered loops and orientated by several disulfide bonds.^{5,47}

According to our results the denaturing process of BSA and BSA–chalcone **3** complex appears to occur by interdomain disruption, followed by the complete unfolding of the protein (helical disruption) in the first and second transitions, respectively. These results are in agreement with those reported for

Table 2 Thermodynamic parameters calculated from the fitted two steps temperature-induced unfolding curves of BSA (5.0×10^{-5} M) in 5 mM Tris-HCl buffer (pH = 7.5) in the presence and absence of chalcone **3** monitored by CD_{222 nm}

Transitions	BSA			BSA–chalcone 3 (2 : 1)		
	First	Second	Total	First	Second	Total
T_m (°C)	64.83 ± 0.17	83.90 ± 0.12	—	70.83 ± 0.13	86.76 ± 0.22	—
ΔH (kcal mol ⁻¹)	28.49 ± 0.13	67.60 ± 0.19	96.09 ± 0.32	45.89 ± 0.18	54.02 ± 0.15	99.91 ± 0.33
ΔS (cal mol ⁻¹ K ⁻¹)	82.46 ± 0.39	192.47 ± 4.07	274.93 ± 4.46	132.20 ± 0.53	153.31 ± 3.45	285.51 ± 3.98
ΔG^{25} (kcal mol ⁻¹)	3.92 ± 0.25	10.24 ± 1.40	14.16 ± 1.65	6.49 ± 0.34	8.33 ± 1.18	14.82 ± 1.52

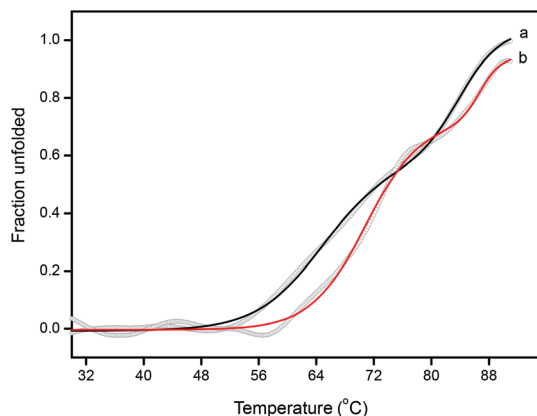


Fig. 11 Temperature induced unfolding curves of 3.0×10^{-7} M of BSA at 5 mM Tris-HCl buffer (pH = 7.5) in the absence (a) and presence (b) of chalcone **3** (1.5×10^{-7} M). Red and black lines correspond to the sigmoidal fitting of experimental data into two transitions states of the BSA unfolding process. These data are calculated considering the changes in molar ellipticities at 222 nm. The inflection points of each sigmoid segment correspond to the melting temperature (T_m) as resumed in Table 2.

fatty acid containing and defatted BSA⁴⁸ and BSA associated with zinc ions,⁴⁹ in which a cooperative unfolding process in the non-two-state model was proposed for the thermal denaturation of BSA in aqueous solution.

A significant difference in the enthalpy and entropy change, estimated from van't Hoff approximation (Fig. 12) for both molecules, was observed in both transitions.

Furthermore, all thermodynamic parameters were higher for the first transition of the BSA–chalcone **3** complex and the second transition of free BSA. However, the final values obtained for the complete unfolding processes were higher for the BSA–chalcone **3** complex (Table 2). Specifically, the thermodynamic parameters for unfolding processes, calculated from that thermal denaturation curves, indicate a remarkable stability of proteins in which the melting temperature of unfolding (T_m) occurs at temperatures above 80.0 °C, like

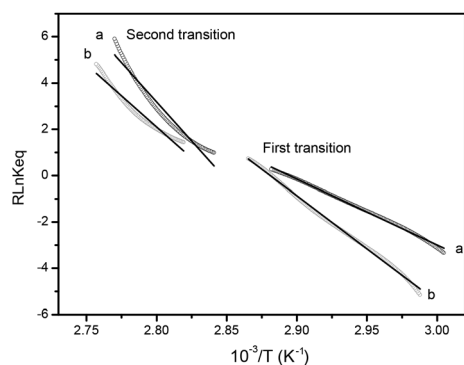


Fig. 12 van't Hoff plot of BSA (3.0×10^{-7} M) at 5 mM Tris-HCl buffer (pH = 7.5) in the absence (a) and presence (b) of chalcone **3** (1.5×10^{-7} M). The experimental and fitted data for the first and second transitions analysed from BSA thermal unfolding curves (see Fig. 11) are represented with the circle symbols and the black lines.

thermophilic globular proteins.^{50,51} Indeed, T_m was higher for the BSA–chalcone **3** complex than for the free BSA protein (Table 2) in both transition phases. This result can also be depicted by the higher value of enthalpy change (ΔH_m about 100.0 kcal mol⁻¹) in the BSA–chalcone **3** complex, indicating a higher structural arrangement of BSA protein upon the formation of the host–guest complex with **3**. The entropy change (ΔS_m) was relatively low for both transition conditions, indicating the predominant contribution of enthalpy change to the Gibbs free energy (ΔG^{25}) of the protein. The values of this parameter (ΔG^{25}) calculated for BSA and the BSA–chalcone **3** complex were 14.16 and 14.82 kcal mol⁻¹, respectively, thus suggesting, by the enthalpy change, a high stability for both molecules at pH 7.5. Despite the stability found for both molecules, altogether the results suggest a higher structural arrangement of BSA in the presence of the guest **3**.

Mass spectrometry analysis

It is well known that chalcone derivatives may undergo intra- and intermolecular Michael additions.^{52–54} Moreover, it has already been described that some enzymes play a role in this reaction.⁵⁵ Thus, it is more than reasonable to envisage a covalent *N*-chalcone bond formation (through a Michael addition) with any nucleophilic amino acid residue inside the BSA binding pocket. It is worth highlighting that until this point, we have assumed non-covalent interactions in the host–guest complex formation.

To make sure that the host–guest overall interaction between BSA and **3** has a non-covalent nature, electrospray ionization quadrupole-time of flight mass spectrometry (ESI-QTOF-MS) experiments were carried out (see Fig. S8† for ESI-QTOF-MS/MS of **3**). Fig. 13 displays mass spectra for BSA electrosprayed under native-like conditions (50 mM ammonium acetate) in the absence (Fig. 13A) or presence (Fig. 13C) of chalcone **3**. Fig. 13B and 13D show, respectively, deconvoluted spectra for BSA in the absence and presence of chalcone **3**.

From the set of spectra obtained, one can observe that the charge state profile of the protein ions changes between samples in which the protein was measured in the absence

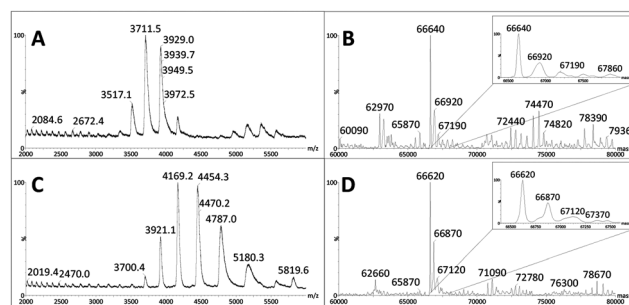


Fig. 13 ESI(+)-QTOF mass spectra for the BSA–chalcone **3** complex. (A) Raw BSA spectrum in the absence of chalcone **3**; (B) deconvoluted BSA spectrum in the absence of chalcone **3**; (C) raw BSA spectrum in the presence of chalcone **3**; (D) deconvoluted spectrum in the presence of chalcone **3**. The insets in spectra (B) and (D) represent expansions around the measured protein mass.

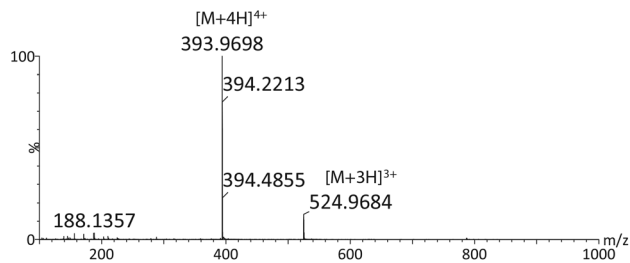


Fig. 14 ESI(+)-QTOF mass spectrum of a sample of peptide Ac-ARAKGAEFVAVKAGVR after treatment with 10 : 1 molar excess of chalcone **3** for 1 h. Note that no signals for peptide–chalcone **3** covalent adducts were observed.

and presence of chalcone **3** (Fig. 13A and 13C), but the measured mass remains the same (Fig. 13B and 13D). This charge state shift demonstrates that BSA changes its conformation upon the binding of chalcone **3**, becoming more tightly folded and thus exposing a lower number of basic residues, leading to a lower charge state distribution. The absence of covalently bonded chalcone **3** molecules, which would appear as a series of peaks with mass shifts of 344 Da (mass of the chalcone derivative), can also be verified in the deconvoluted spectra.

Since BSA is a protein of ≈ 66.500 Da, we decided to evaluate the interaction of chalcone derivative **3** with a smaller biomolecule such as a peptide. In the experiment, we used peptide

Ac-ARAKGAEFVAVKAGVR that contains two nucleophilic lysine residues, which was treated with 10 : 1 molar excess of chalcone **3** (100 mM sodium carbonate/bicarbonate buffer media; pH = 9.5). The lower mass of the peptide (when compared with BSA) would allow a better visualization of any covalent interaction through any *N*-chalcone bond formation. Even after 1 hour of reaction, no covalent adduct between the peptide and chalcone derivative could be observed, as shown in Fig. 14.

Overall, mass spectrometry experiments demonstrated that no covalent bond is formed between BSA and **3**; thus it is in full accordance with the assumption of non-covalent interaction between BSA and **3**. Moreover, it demonstrates that BSA changes its conformation upon the binding of chalcone **3**, becoming more tightly folded.

NMR experiments and analyses

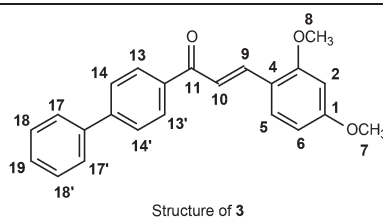
^1H -, ^{13}C -, 1D and 2D gs-HSQC and gs-HMBC experiments were applied to a complete and undoubtedly chemical shift assignment of chalcone **3** before and after BSA addition to the solution (see Fig. S9 and S10 in the ESI†).

^1H and ^{13}C chemical shifts of **3** are summarized in Table 3. Fig. 15 shows the ^1H and expanded ^{13}C NMR titration experiments of chalcone **3** with BSA.

^{13}C NMR (see the whole spectra in Fig. S11†) showed an interesting shift on the $\text{C}=\text{O}$ signal and a deshielded effect of

Table 3 ^1H and ^{13}C NMR assignments (chemical shift in ppm) for chalcone **3** (200 mM) in the absence and presence of BSA (15 μM) in DMSO-d_6

Position	3		3 + BSA		Differences in ppm (3 + BSA)- 3	
	^1H	^{13}C	^1H	^{13}C	ΔH	ΔC
1	—	163.2	—	163.2	—	—
2	6.67 (s, 1H)	98.4	6.65 (m, 1H)	98.2	0.02	-0.2
3	—	160.1	—	160.1	—	—
4	—	116.1	—	115.9	—	-0.2
5	7.96 (m, 1H)	130.3	7.91 (m, 1H)	130.3	0.05	—
6	6.64 (m, 1H)	106.5	6.67 (m, 1H)	106.5	0.03	—
7	3.86 (s, 3H)	55.6	3.86 (s, 3H)	55.6	—	—
8	3.92 (s, 3H)	55.9	3.92 (s, 3H)	55.9	—	—
9	8.05 (d, 15.7 Hz, 1H)	138.9	8.05 (d, 15.7 Hz, 1H)	139.1	—	0.2
10	7.83 (d, 15.7 Hz, 1H)	119.1	7.80 (d, 15.7 Hz, 1H)	118.9	0.03	-0.2
11	—	188.7	—	189.0	—	0.3
12	—	136.9	—	136.8	—	-0.1
13 and 13'	8.20 (m, 2H)	129.2	8.18 (m, 2H)	129.1	0.02	-0.1
14 and 14'	7.85 (m, 2H)	127.1	7.85 (m, 2H)	127.0	—	-0.1
15	—	144.3	—	144.3	—	—
16	—	139.1	—	138.9	—	-0.2
17 and 17'	7.77 (m, 2H)	127.0	7.77 (m, 2H)	127.0	0.01	—
18 and 18'	7.52 (m, 2H)	129.2	7.53 (m, 2H)	129.1	—	-0.1
19	7.44 (m, 1H)	128.5	7.45 (m, 1H)	128.5	0.01	—



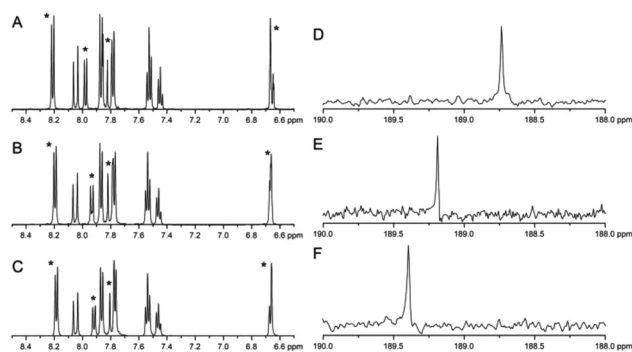


Fig. 15 ^1H NMR spectra of (A) a 200 mM solution of **3** in DMSO-d_6 , (B) with 10 μM and (C) with 15 μM of BSA. *signals with changes in their chemical shift. ^{13}C NMR spectra of (D) 200 mM solution of **3** in DMSO-d_6 , (E) with 10 μM and (F) with 15 μM of BSA.

0.3 ppm was noticed (Fig. 15, right). C=C carbons also suffered a chemical shift variation. Interestingly, the carbon at C9 position deshielded (0.2 ppm) while the carbon at C10 shielded (0.2 ppm). These carbons (C=C-C=O – the Michael system) were expected to suffer the most pronounced effect upon protein binding and, as predicted, these are among the most significant changes. Some carbons at the electron-rich phenyl ring (C2 and C4) also displayed a small shield as a consequence of both the interaction with BSA and the disturbance in the Michael π -system. ^1H NMR chemical shift variations for free chalcone **3** and BSA-bound complex revealed some preferred interaction sites between the host and guest (Table 3). In the presence of BSA, ^1H NMR chemical shifts of H2, H5, H10 and H13/H13', H18/H18' and H19 were shielded while H6 was deshielded. The observed changes in the chemical shifts point firmly towards different local environment reflections as a consequence of the host-guest interactions (BSA-chalcone **3** complex formation). Importantly, the H9 chemical shift, which is involved in the Michael system, does not change in the ^1H NMR experiment, in accordance with its non-covalent interaction nature. H5 and H6, however, showed preminent changes (see Table 3). In addition, the methoxy group at C1, which is relatively close to H5 and H6 of structure **3**, also showed a considerable change in the chemical shift, thus suggesting that the enzyme interaction takes place preferentially on this side of the fluorescent probe.

When ^{13}C NMR chemical shift variations are analyzed, it is evident that C2, C4, C10, C12, C13/C13', C14/C14', C16, and C18/C18' were shielded. Interestingly, C9 and C11 (both Michael system) were deshielded, indicating a decrease in electronic density experienced by these atoms, most likely due to the induced interaction with a BSA hydrophobic pocket. Once more, the small chemical shift variation of these carbons show the non-covalent nature of the interaction upon host-guest complex formation. Except for C2, the chemical shift of an aromatic ring with the methoxy substituents did not present differences in the chemical shift. On the other hand, the chemical surrounding of most carbon atoms of the biphenyl group (except for C15, C17, C19) showed a considerable

change in their chemical shifts. This result corroborates with fluorescence data and indicates the interaction of this motif with the protein. Note, once more, that these results are in full accordance with the suggested preferential side of interaction of the host with BSA.

NMR relaxation time measurements (T_1 and/or T_2) experiments could also be performed because they are among the most suitable tools to probe binding processes at the molecular level. In this sense, both techniques could be carried out to study the current interactions. ^1H T_1 relaxation times were measured for the free dye **3** and upon BSA addition. These results were not conclusive since observed changes in T_1 data were too small to be significant (see Table S1†), despite the fact that these data point in the same direction of the analyzed chemical shifts.

In order to obtain more conclusive and reliable information with relaxation time measurements, ^{13}C T_1 relaxation time experiments were then carried out in the absence and presence of the host biomolecule. All results are summarized in Table 4.

Upon BSA addition, it is noted that there are substantial changes in the ^{13}C T_1 relaxation times when compared with those observed for the free chalcone **3**. Results showed that ^{13}C T_1 decreased significantly for 4C and 11C. The relaxation process occurs *via* a transfer from the nucleus to the surrounding (lattice) and the ^{13}C nucleus relaxes predominantly *via* a dipole-dipole mechanism to the covalently attached hydrogens. Interestingly, a more prominent decrease in T_1 relaxation times occurred in the quaternary nucleus. This is strong evidence that a faster relaxation process is being stimulated by the interaction of these nuclei with the protein, thus providing a qualitative insight into the site-specific binding of **3** to BSA. This is in accordance with the previous NMR analyses already discussed. For all other carbons, it is noted that there are just small changes in the T_1 values, clearly indicating a weaker contact with the macromolecule interaction domain.

Table 4 ^{13}C T_1 (s) of chalcone **3** (200 mM) in the absence and after the addition of BSA to form 5 μM , 10 μM and 15 μM solutions of the host biomolecule

Position	Guest 3	3 + BSA (5 μM)	3 + BSA (10 μM)	3 + BSA (15 μM)
1	3.38	3.16	3.04	2.94
2	0.26	0.30	0.31	0.22
3	4.38	4.62	4.87	4.07
4	5.08	5.15	2.95	3.81
5	0.27	0.24	0.30	0.22
6	0.39	0.31	0.28	0.28
7	0.92	1.07	1.29	0.86
8	0.74	0.79	0.74	0.60
9	0.38	0.35	0.39	0.35
10	0.36	0.38	0.31	0.34
11	4.12	2.47	2.89	2.29
12	3.58	2.93	2.29	2.88
13 and 13'	0.61	0.59	0.55	0.57
14 and 14'	0.60	0.61	0.50	0.57
15	2.48	2.58	2.95	2.47
16	3.08	3.07	2.37	—

Theoretical calculations

To characterize the reactivity and photophysical behavior of the fluorescent chalcone **3**, DFT calculations were performed since it has been previously shown to be a useful approach to understand the solvent–chalcone interactions, absorptions bands, emissions processes and the stabilizing ICT process for a chalcone derivative.⁵⁶ Water was also used as the medium for the simulations as a prelude to cellular experiments and mostly because it is the natural enzyme medium.

Chalcone **3** had its structure optimized in the ground (S_0) and excited (S_1) states at B3LYP/6-311+g(2d,p) level of calculations. The optimized geometries of S_0 and S_1 were used for the single point calculations at the (TD-)PBE1PBE/6-311+g(2d,p) level of calculations. Absorption spectra in close agreement with experiments have been obtained using the TD-PBE1PBE/6-311+G(2d,p) level of calculation. Optimized geometries are also shown considering water as a solvent (Fig. 16).

Chalcone **3** showed a tendency to sustain its conformation in the ground and in the excited states (Fig. 16). When the structure was simulated in water, similar results were obtained, indicating that the aqueous media will not exert a significant influence on the geometry of the molecule, even in the excited state. It is of interest to note the preferred position of the methyl group for the second methoxy substituent (Fig. 17).

It was noticed that in the optimized geometries the hydrogens of the O–CH₃ group (at C1) are positioned close to the hydrogens at C6 and C5. It is expected that upon interacting

with the protein, the molecular motion decreases; then the effect in the NMR should be more pronounced in the hydrogens (and carbons) close to the protein pocket. As discussed before, it was noticed that there is an enhanced NMR effect, especially for ¹³C T_1 relaxation time experiments.

As shown before, the Stokes shift in the titrations experiments (≈ 100 nm) is similar to that in methanol, thus showing that the polar and the protic medium contribute to stabilizing the dye in the excited state. Furthermore, large Stokes shifts suggest orbital and dipole moment changes in the excited state compared with the ground state.³² Such differences agree with the changes from the Franck–Condon state.⁵⁷ To verify these observations, we calculated both the orbital behaviour and the changes in the dipole moment (also related with the efficiency of the ICT process).

The previously optimized structure had its HOMO and LUMO orbitals evaluated in the ground and excited state. Moreover, the same orbitals were also analysed considering water as a solvent. Interestingly, in the presence or absence of water (solvent effect), the chalcone showed a similar orbital distribution (Fig. 18).

For all situations the phase of the HOMO orbitals is concentrated in the methoxyphenyl side, whereas the LUMO are more distributed, but clearly show a tendency towards the conjugated C=C–C=O moiety of the structure (Michael system). Also, as depicted in Fig. 18, both HOMO and LUMO are of π type.

In simulations in vacuum, we observed that HOMO orbitals showed a similar distribution in the ground (S_0) and excited (S_1) states. LUMO orbitals did not show any significant change as well. Note again that the HOMO electronic map distribution is basically on the phenyl moiety with the methoxy substituents

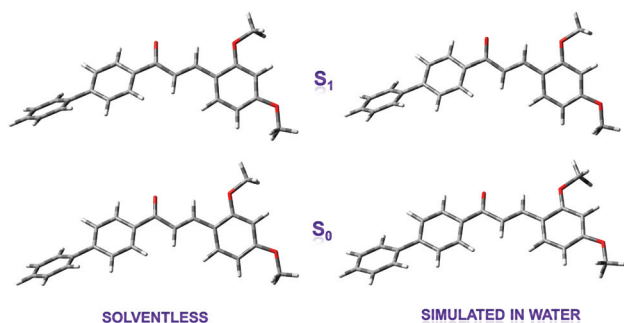


Fig. 16 Optimized geometries of chalcone **3** in the ground and excited states in both vacuum and aqueous solvent. (Left) Vacuum and (Right) considering the solvent effect (simulated in water). Results obtained at the B3LYP/6-311+g(2d,p) level of calculations.

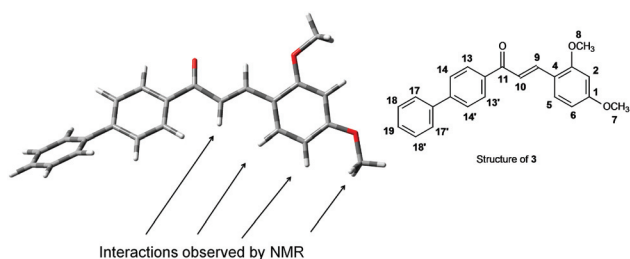


Fig. 17 Optimized geometries of chalcone **3** at the ground state to highlight the hydrogen interactions observed by NMR experiments.

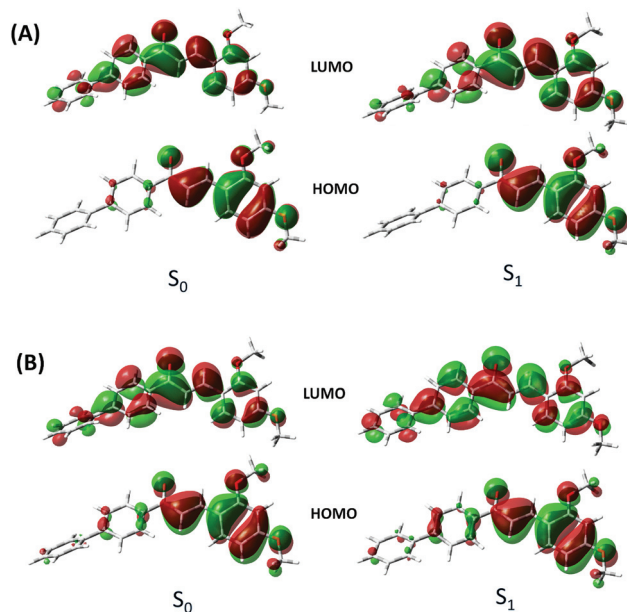
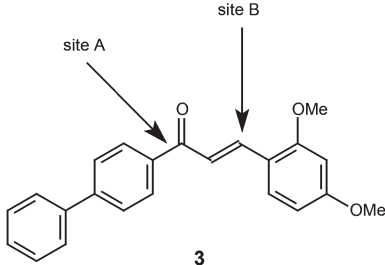


Fig. 18 Molecular orbital plots (HOMO and LUMO) of the fluorescent chalcone **3** for both the ground and the first excited states. (A) Solventless and (B) considering the solvent effect (simulated in water).

Table 5 Condensed Fukui function (f^+ values) for the expected reaction sites of the fluorescent chalcone **3**


State (ground or first excited)	Fukui function values (f^+)	
	Site A	Site B
S_0	0.13	0.11
S_1	0.11	0.14
S_0 (in water)	0.15	0.13
S_1 (in water)	0.12	0.10

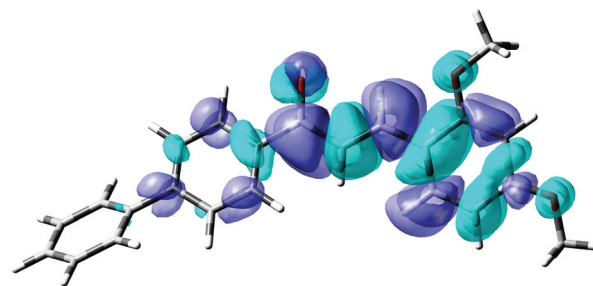
whereas the LUMO orbitals are on the C=O, as expected and discussed before (also see Fig. 2 for the accepting moiety).

Experiments simulated in water gave very interesting results. Indeed, no significant change could be noted when comparing the experiments in the presence and absence of water. This clearly suggests that the fluorescent chalcone has a weak affinity for water. Therefore, it is expected that the dye will interact with the hydrophobic part of the protein, *i.e.* it is expected that the probe will be found surrounded by hydrophobic pockets of the macromolecule (BSA), as already indicated by the value of the Stern–Volmer constant. In this sense, the calculations described herein are in full accordance with the experimental data.

Condensed Fukui functions (f^+ values) were also calculated to indicate the preferential site of interaction of the fluorescent probe and the protein. Values for the selected sites are shown in Table 5. Table S2 in the ESI† shows the calculated values for all carbon atoms.

The calculated condensed Fukui values indicate that both sites (A and B) may preferentially interact with the protein. The described values were the largest among all those calculated for the optimized structure of derivative **3**. Moreover, as demonstrated by NMR experiments, these are some of the preferred sites for the guest (chalcone **3**) interaction with the host (BSA). It was noted that those values are quite close independent of whether in the ground or in the excited state. Once more, the theoretical calculations are in full accordance with the experimental data. It is also noteworthy that these values are not very high; thus it is reasonable to discard a new covalent bond formation upon any reaction with an amino acid residue from the protein and, once more, this theoretical experiment is in full accordance with the experimental data, *i.e.* the mass spectrometry experiments, as discussed before.

In order to probe the efficiency of the stabilizing ICT process, the dipole moment (ground and excited states) was calculated for chalcone derivative **3** and an electron density

**Fig. 19** Electron density difference computed for the ground and excited states for the fluorescent probe **3**. Purple represents the state before the charge-transfer and green represents the state after the process. Note that before the process the electron density is in the methoxy groups (purple) and after the process it is in the C=O (light green).

difference map (Fig. 19) could be calculated, *i.e.* the differential charge densities ($\Delta\rho$) between the excited and the ground state ($\Delta\rho = \rho(S_1) - \rho(S_0)$). Fig. 19 shows a dynamic visualization of the electronic rearrangements for the expected transition. The purple regions (positive values) denote an accumulation of density, whereas the green regions (negative values) represent a depletion of density upon excitation. In support of the assertion of a charge transfer nature process, it is noted that positive values (purple) are concentrated in the phenyl ring with methoxy substituents, while close (spatial proximity) negative values (light green) are noted in the C=C–C=O region (Michael system). With all the data already presented, it is more than reasonable to suggest that in the excited state chalcone **3** has a clear preference for an ICT process rather than undergoing any Michael addition reaction. Once more, these results are in accordance with the mass spectrometry experiments already discussed.

The difference in the dipole moment was calculated and also indicated the efficiency of the ICT process and, once more, it is in full accordance with the results previously presented and discussed in Table 1. The dipole moment in vacuum is 4.89 D (ground state) and 6.39 D (excited state). In the aqueous medium those values change to 7.30 D and 8.08 D, respectively. The observed difference is in full accordance with the expected ICT process to stabilize the fluorescent probe **3** in the excited state through a direct charge transfer from the methoxyphenyl groups to the carbonyl group. Altogether, these results indicate that the designed molecular architecture of chalcone **3** plays a role in the stabilization of the molecule in the excited state, thus rendering this probe one of the most efficient ever described to study host–guest interactions of chalcones and proteins.

In order to identify the binding sites and predominant binding conformations of chalcone **3** upon interaction with BSA, molecular docking calculations were performed. Molecular docking methods provide a well-established approach to rank potential ligands with respect to their ability to interact with a given target.^{58,59} It involves the efficient sampling of possible poses of small molecules in the specified binding pocket of a protein in order to identify the optimal binding geometry, as measured by a score function.

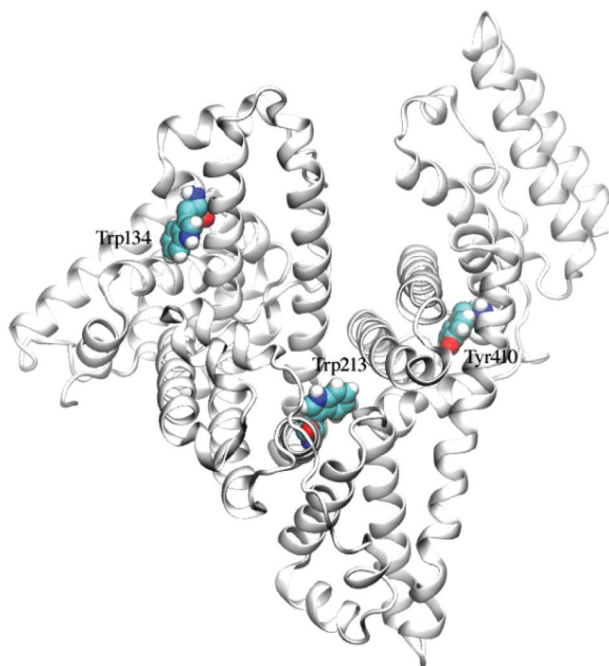


Fig. 20 Cartoon representation of the X-ray structure of BSA. Proposed binding sites for chalcone derivatives are indicated by residues Trp134 (domain I), Trp213 (domain II) and Tyr 410 (domain III).

The BSA biomolecule has three homologous domains (I, II, III), each one being composed of two subdomains (IA, IB, IIA, IIB, IIIA and IIIB). In the widely studied human serum albumin (HSA), subdomains IIA and IIIA are the favoured binding regions for aromatic and heterocyclic ligands, as already demonstrated.^{60–62} Therefore, we have searched these regions for favourable binding sites for chalcone **3** *via* molecular docking calculations. BSA has two tryptophan residues, which have been linked to the intrinsic fluorescence associated with this protein (Fig. 20). Our docking calculations show that residues Trp134 (site A) and Trp213 (site B) are the most favourable binding sites for chalcone **3** (Fig. 21 and 22).

It is worth highlighting that by using circular dichroism, it was also noted that there are two favourable binding sites for chalcone **3**, once more in accordance with the experimental results.

Trp134 is located in a shallow cleft on the surface of domain I, which is protected from the solvent by salt-bridges formed by residues Glu17 and Lys131 in the absence of the ligand (Fig. 21). Trp213 is located within a deeper pocket in domain II, connected to the protein surface by a hydrophobic channel (Fig. 22). Our results indicate that chalcone **3** can bind to both tryptophan sites with an affinity constant of the order of μM . This is consistent with previous studies where an analogous compound, namely licochalcone A, was shown to associate with two BSA sites of similar affinity.³ Moreover, it is also consistent with the calculated constants (circular dichroism) presented herein. And once more, it is in accordance with a 3 : 1 chalcone–BSA proportion found using spectroscopic analyses. The most populated conformational cluster for

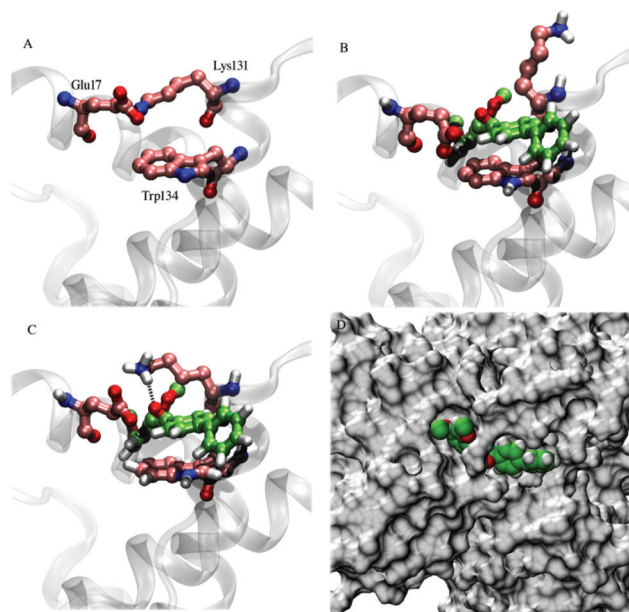


Fig. 21 Representation of Trp134 binding site (A) in the X-ray structure, (B) after the molecular docking with flexible treatment of Glu17, Lys131 and Lys 132, (C) after molecular dynamic simulations in explicit solvent, and (D) in the molecular surface of the protein.

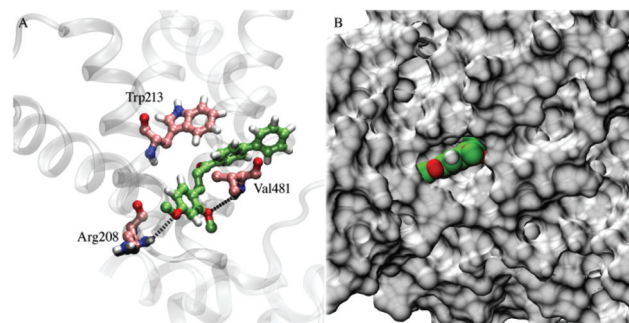


Fig. 22 Representation of Trp213 binding site (A) after molecular dynamic simulations in explicit solvent, and (B) in the molecular surface of the protein.

binding to site A and site B represented 95% and 34%, respectively, of the lowest energy conformers (out of a total of $ca. 4 \times 10^8$ sampled conformations). The lowest energy conformations bind to site A and site B with interaction energies of $ca. -5.4 \text{ kcal mol}^{-1}$ to $-5.5 \text{ kcal mol}^{-1}$.

Chalcone **3** binds to Trp213 (site B) through the stacking of aromatic rings in a so-called T-shape configuration (Fig. 22A). The methoxy groups interact *via* weak hydrogen bonds to residues Val481 (backbone amide group) and Arg208 (side-chain guanidinium group, Fig. 22A). Upon binding, the biphenyl group of chalcone **3** becomes fully buried in the hydrophobic channel leading to the Trp213 pocket (Fig. 22B), in accordance with circular dichroism, fluorescence and NMR experiments. Only carbon C2 in the third benzene ring, carbon C8 in one of the methoxy groups, and the oxygen bonded to carbon C7 in the other methoxy group remain fairly accessible to the solvent upon ligand binding to the Trp213 (site A) (Fig. 22B).

The existence of a second binding site was not obvious from simple visual inspection of the BSA crystallographic structure. The first docking attempts to bind chalcone **3** to site A were, indeed, unsuccessful. Only after considering the residues Glu17 and Lys131 fully flexible during the docking calculations, it was possible to dock chalcone **3** to this site (Fig. 21A and 21B). Chalcone **3** binds to Trp134 through the stacking of aromatic rings in a parallel-displaced configuration (Fig. 21B). Due to the shallowness of the Trp134 site, the biphenyl group remains fairly exposed to the solvent upon binding (Fig. 21D). Our MD simulations showed that there is a conformational rearrangement of Lys131 upon ligand binding to site A. This residue forms a hydrogen bond to the carbonyl group of chalcone **3**, thus locking the ligand in place upon binding to BSA (Fig. 21C). These findings suggest that chalcone **3** binding to site A is strongly dependent on a “gate opening” mechanism that may result in a slower ligand association rate when compared to site II (Fig. 21). Once again, theoretical and experimental data are in accordance, and the predicted binding conformations are very consistent with the chemical shift measurements performed for chalcone **3** bound to BSA (also see Tables 3 and 4). Accordingly, atoms C2, H2, O7 (in the first OCH₃ group) and C8 (in the second OCH₃ group) remain fairly exposed to the solvent upon ligand binding with both sites.

The association between licochalcone A and BSA has been previously studied through a combination of spectroscopic, photophysical and computational approaches.³ It has shown that licochalcone A preferentially binds to two protein sites which have been assigned to residues Trp213 and Tyr410 by means of molecular docking calculations (note that we refer to the residue sequence number from the PDB structure (3V03) rather than the sequence number used elsewhere³). Actually, chalcone **3** and the licochalcone A have both an electron rich phenyl ring (despite the structural difference); thus it is reasonable to expect some similar interactions upon binding to the same site in BSA. Indeed, the binding site corresponding to Trp213 is the same for both ligands (licochalcone A and **3**). The second binding site, however, was suggested to be Tyr410 for licochalcone A, while in the meantime it is proposed to be Trp134 for chalcone **3**. To address this apparent discrepancy, and in order to discard the possibility of Tyr410 interaction with **3**, we have performed additional docking calculations aiming specifically at this region. The calculations indicated that chalcone **3** can bind to the hydrophobic pocket containing Tyr410 in two predominant conformations with an interaction energy of *ca.* -4.5 kcal mol⁻¹ (Fig. 23).

Despite the less favourable interaction energy of chalcone **3** to Tyr410 compared to Trp134 and Trp213, the difference between the respective binding energies is within the error associated with our score function, which cannot reliably discriminate between these binding sites.³ However, the binding conformations of chalcone **3** in the Tyr410 site have the methoxy-aromatic system either fully exposed to the solvent or fully buried within the hydrophobic pocket. Such an interaction pattern is conflicting with the chemical shift

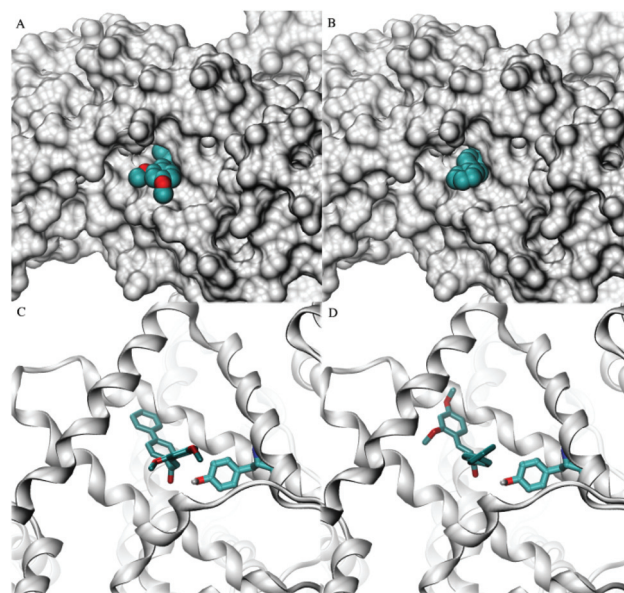


Fig. 23 Predominant binding conformations of chalcone **3** to Tyr410. (A, C) Conformation I corresponds to 38% and (B, D) conformation II to 27% of the lowest energy conformers (out of a total of *ca.* 8×10^8 sampled conformations) respectively.

measurements for chalcone **3** upon binding to BSA, showing that only part of the atoms in the methoxy-aromatic system interact with BSA. Therefore, the discussed NMR measurements associated with the computational calculations indicate that Tyr410 is not a major binding site for chalcone **3**. It is also possible that some discrepancies in the BSA three-dimensional structure used in the two computational studies could explain, at least in part, these conflicting findings. In our study the crystallographic structure of BSA (PDB ID 3V03) was used whereas the docking of licochalcone A was performed for a homology-based structural model built from the crystallographic structure of HSA, which shares about 77% sequence identity with BSA.³ Local variations in the position of side-chains can affect significantly the docking predictions since the protein structure is kept rigid during the calculations, unless some residues are chosen to be treated as flexible. Nevertheless, further experimental measurements will be required to undoubtedly ascertain the second binding site of chalcone derivatives to BSA. Despite this apparent conflict, the data from NMR, circular dichroism and fluorescence indicate that two major binding sites are preferred, *i.e.* Trp134 and Trp213, as shown herein.

Conclusions

A novel rationally designed fluorescent chalcone derivative was efficiently synthesized and applied as a probe to study the host-guest interactions with BSA. The photophysical properties showed that the new derivative is highly stable and is stabilized in the excited state by an efficient ICT process. Spectrophotometric and spectrofluorimetric titrations showed that

the interaction takes place preferentially in the hydrophobic region of the protein. NMR experiments showed the preferred site of interaction of chalcone 3 with the protein. It is worth noting, based on circular dichroism experiments, that the stability of biological and chemical molecules is a fundamental feature aiming clinical and biotechnological applications. In this work, the results obtained from structural studies of the BSA–chalcone 3 binding process, based on thermal denaturant effects, can be useful also to predict the stability of this complex in the human blood vessel. Moreover, the results are in accordance with two possible binding sites. ESI-MS showed the non-covalent nature of the host–guest interaction. ^1H NMR and ^{13}C T_1 relaxation time experiments gave very interesting results and demonstrated which atoms of 3 were suffering a major influence of the protein through the host–guest interactions. Theoretical calculations revealed the preference for hydrophobic regions of the fluorescent probe and showed the preferred sites of interaction in full accordance with the experimental analyses. Additionally, it corroborates with the efficiency of the ICT process to stabilize the dye in the excited state. Molecular docking calculations were used to identify the sites of interaction (two preferential sites) between BSA and chalcone 3, showing a preference to interact with tryptophan residues Trp134 (site A) and Trp213 (site B). Finally, all features of the designed dye indicate that this is one of the most efficient probes ever described to be used as a model in the host–guest interactions of chalcones and proteins. Moreover, it opens up a new avenue towards a rational design for new fluorescent chalcone derivatives to be used in this kind of study.

Notes and references

- 1 A. A. Marti, S. Jockusch, N. Stevens, J. Y. Ju and N. J. Turro, *Acc. Chem. Res.*, 2007, **40**, 402–409.
- 2 M. M. Kemp, M. Weiwer and A. N. Koehler, *Bioorg. Med. Chem.*, 2012, **20**, 1979–1989.
- 3 S. Monti, I. Manet, F. Manoli, S. Ottani and G. Marconi, *Photochem. Photobiol. Sci.*, 2009, **8**, 805–813.
- 4 S. Monti, I. Manet, F. Manoli and G. Marconi, *Phys. Chem. Chem. Phys.*, 2008, **10**, 6597–6606.
- 5 T. Peters, *Adv. Protein Chem.*, 1985, **37**, 161–245.
- 6 Meetu and N. Raghav, *Asian J. Chem.*, 2009, **21**, 5475–5482.
- 7 S. Monti, F. Manoli, S. Sortino, R. Morrone and G. Nicolosi, *Phys. Chem. Chem. Phys.*, 2005, **7**, 4002–4008.
- 8 S. Monti, I. Manet, F. Manoli, R. Morrone, G. Nicolosi and S. Sortino, *Photochem. Photobiol.*, 2006, **82**, 13–19.
- 9 S. Monti, I. Manet, F. Manoli and S. Sortino, *Photochem. Photobiol. Sci.*, 2007, **6**, 462–470.
- 10 L. M. Ni, C. Q. Meng and J. A. Sikorski, *Expert Opin. Ther. Pat.*, 2004, **14**, 1669–1691.
- 11 Z. Nowakowska, *Eur. J. Med. Chem.*, 2007, **42**, 125–137.
- 12 N. K. Sahu, S. S. Balbhadra, J. Choudhary and D. V. Kohli, *Curr. Med. Chem.*, 2012, **19**, 209–225.
- 13 W. Y. He, Y. Li, J. Q. Liu, Z. D. Hu and X. G. Chen, *Biopolymers*, 2005, **79**, 48–57.
- 14 K. Rurack, M. L. Dekhtyar, J. L. Bricks, U. Resch-Genger and W. Rettig, *J. Phys. Chem. A*, 1999, **103**, 9626–9635.
- 15 M. K. Saroj, N. Sharma and R. C. Rastogi, *J. Mol. Struct.*, 2012, **1012**, 73–86.
- 16 M. Danko, A. Andics, C. Kosa, P. Hrdlovic and D. Vegh, *Dyes Pigm.*, 2012, **92**, 1257–1265.
- 17 T. A. Fayed and M. K. Awad, *Chem. Phys.*, 2004, **303**, 317–326.
- 18 T. Suwunwong, S. Chantrapromma and H. K. Fun, *Chem. Pap.*, 2011, **65**, 890–897.
- 19 S. C. Lee, N. Y. Kang, S. J. Park, S. W. Yun, Y. Chandran and Y. T. Chang, *Chem. Commun.*, 2012, **48**, 6681–6683.
- 20 B. A. D. Neto, A. A. M. Lapis, F. S. Mancilha, I. B. Vasconcelos, C. Thum, L. A. Basso, D. S. Santos and J. Dupont, *Org. Lett.*, 2007, **9**, 4001–4004.
- 21 B. A. D. Neto, A. A. M. Lapis, F. S. Mancilha, E. L. Batista, P. A. Netz, F. Rominger, L. A. Basso, D. S. Santos and J. Dupont, *Mol. BioSyst.*, 2010, **6**, 967–975.
- 22 B. A. D. Neto and A. A. M. Lapis, *Molecules*, 2009, **14**, 1725–1746.
- 23 B. A. D. Neto, P. H. P. R. Carvalho, D. C. B. D. Santos, C. C. Gatto, L. M. Ramos, N. M. de Vasconcelos, J. R. Corrêa, M. B. Costa, H. C. B. de Oliveira and R. G. Silva, *RSC Adv.*, 2012, **2**, 1524–1532.
- 24 B. A. D. Neto, J. R. Correa, P. Carvalho, D. Santos, B. C. Guido, C. C. Gatto, H. C. B. de Oliveira, M. Fasciotti, M. N. Eberlin and E. N. da Silva, *J. Braz. Chem. Soc.*, 2012, **23**, 770–781.
- 25 C. K. Z. Andrade and W. A. Silva, *Lett. Org. Chem.*, 2006, **3**, 39–41.
- 26 W. A. Silva, C. C. Gatta and G. R. Oliveira, *Acta Crystallogr. Sect. E: Struct. Rep. Online*, 2011, **67**, O2210–U1525.
- 27 G. R. de Oliveira, H. C. B. de Oliveira, W. A. Silva, V. H. C. da Silva, J. R. Sabino and F. T. Martins, *Struct. Chem.*, 2012, **23**, 1667–1676.
- 28 F. J. Zhang, X. Wu and J. H. Zhan, *J. Fluoresc.*, 2011, **21**, 1857–1864.
- 29 Y. Imai, K. Komon, N. Tajima, T. Kinuta, T. Sato, R. Kuroda and Y. Matsubara, *J. Lumin.*, 2010, **130**, 954–958.
- 30 K. Medjanik, D. Chercka, P. Nagel, M. Merz, S. Schuppler, M. Baumgarten, K. Mullen, S. A. Nepijko, H. J. Elmers, G. Schonhense, H. O. Jeschke and R. Valenti, *J. Am. Chem. Soc.*, 2012, **134**, 4694–4699.
- 31 R. Baskar and K. Subramanian, *Spectrochim. Acta, Part A*, 2011, **79**, 1992–1997.
- 32 G. Ulrich, F. Nastasi, P. Retailleau, F. Puntoriero, R. Ziessel and S. Campagna, *Chem.–Eur. J.*, 2008, **14**, 4381–4392.
- 33 P. Perjesi, K. Fodor and T. Koszegi, *Eur. J. Pharm. Sci.*, 2007, **32**, S38–S39.
- 34 C. Reichardt, *Chem. Rev.*, 1994, **94**, 2319–2358.
- 35 P. Rajakumar, A. Thirunarayanan, S. Raja, S. Ganesan and P. Maruthamuthu, *Tetrahedron Lett.*, 2012, **53**, 1139–1143.
- 36 S. H. Mashraqui, S. Sundaram and T. Khan, *Chem. Lett.*, 2006, 786–787.

- 37 H. J. Ravindra, A. J. Kiran, S. M. Dharmaprasanth, N. S. Rai, K. Chandrasekharan, B. Kalluraya and F. Rotermund, *J. Cryst. Growth*, 2008, **310**, 4169–4176.
- 38 C. J. Tonzola, M. M. Alam, W. Kaminsky and S. A. Jenekhe, *J. Am. Chem. Soc.*, 2003, **125**, 13548–13558.
- 39 A. Granzhan and H. Ihmels, *Org. Lett.*, 2005, **7**, 5119–5122.
- 40 A. Granzhan, H. Ihmels and G. Viola, *J. Am. Chem. Soc.*, 2007, **129**, 1254–1267.
- 41 K. Fodor, V. Tomescova, T. Koszegi, I. Kron and P. Perjesi, *Monatsh. Chem.*, 2011, **142**, 463–468.
- 42 H. M. S. Kumar, R. S. Kunabenchi, J. S. Biradar, N. N. Math, J. S. Kadadevarmath and S. R. Inamdar, *J. Lumin.*, 2006, **116**, 35–42.
- 43 C. Bertucci and E. Domenici, *Curr. Med. Chem.*, 2002, **9**, 1463–1481.
- 44 J. T. Pelton and L. R. McLean, *Anal. Biochem.*, 2000, **277**, 167–176.
- 45 D. H. A. Correa and C. H. I. Ramos, *Afr. J. Biochem. Res.*, 2009, **3**, 164–173.
- 46 C. N. Pace, *Trends Biochem. Sci.*, 1990, **15**, 14–17.
- 47 X. M. He and D. C. Carter, *Nature*, 1992, **358**, 209–215.
- 48 A. Michnik, *J. Therm. Anal. Calorim.*, 2003, **71**, 509–519.
- 49 S. Ostojic, V. Dragutinovic, M. Kicanovic and B. R. Simonovic, *J. Serb. Chem. Soc.*, 2007, **72**, 331–337.
- 50 S. Kumar, C. J. Tsai and R. Nussinov, *Protein Eng.*, 2000, **13**, 179–191.
- 51 S. Kumar, C. J. Tsai and R. Nussinov, *Biochemistry*, 2001, **40**, 14152–14165.
- 52 C. E. Paul, V. Gotor-Fernandez, I. Lavandera, J. Montejó-Bernardo, S. Garcia-Granda and V. Gotor, *RSC Adv.*, 2012, **2**, 6455–6463.
- 53 M. Moccia, F. Fini, M. Scagnetti and M. F. A. Adamo, *Angew. Chem., Int. Ed.*, 2011, **50**, 6893–6895.
- 54 S. Kobayashi and Y. Yamashita, *Acc. Chem. Res.*, 2011, **44**, 58–71.
- 55 M. N. Ngaki, G. V. Louie, R. N. Philippe, G. Manning, F. Pojer, M. E. Bowman, L. Li, E. Larsen, E. S. Wurtele and J. P. Noel, *Nature*, 2012, **485**, 530–U147.
- 56 Y. S. Xue, L. An, Y. G. Zheng, L. Zhang, X. D. Gong, Y. Qian and Y. Liu, *Comput. Theor. Chem.*, 2012, **981**, 90–99.
- 57 A. U. Khan and M. Kasha, *Proc. Natl. Acad. Sci. U. S. A.*, 1983, **80**, 1767–1770.
- 58 W. L. Jorgensen, *Acc. Chem. Res.*, 2009, **42**, 724–733.
- 59 N. Brooijmans and I. D. Kuntz, *Annu. Rev. Biophys. Biomol. Struct.*, 2003, **32**, 335–373.
- 60 M. Dockal, M. Chang, D. C. Carter and F. Ruker, *Protein Sci.*, 2000, **9**, 1455–1465.
- 61 G. Sudlow, D. J. Birkett and D. N. Wade, *Mol. Pharmacol.*, 1976, **12**, 1052–1061.
- 62 D. Agudelo, P. Bourassa, J. Bruneau, G. Berube, E. Asselin and H. A. Tajmir-Riahi, *PLoS One*, 2012, **7**, e43814.